La Metallurgia Italiana
International Journal of the Italian Association for Metallurgy

DOI 10.36146/2026_05_27

Effects of synthesis parameters on the properties of iron nanoparticles synthesized via the borohydride method

Tien Hiep Nguyen, Ho Thanh Nghi, Nguyen Van Minh, Nguyen Manh Hung

This study investigates the influence of solution pumping speed and ultrasonic wave amplitude on the properties of iron nanoparticles synthesized via the borohydride reduction method of iron (II) sulfate ($FeSO_4$) and iron (III) chloride ($FeCl_3$) precursor solutions. The results indicate that combining a high-amplitude ultrasonic wave with a high $NaBH_4$ solution pumping speed yields nanoparticles with an optimal size distribution and improved dispersion in both cases. Iron nanoparticles synthesized from iron (II) sulfate ($FeSO_4$) exhibited better size uniformity and dispersion compared to those synthesized from iron (III) chloride ($FeCl_3$). In both cases, the iron nanoparticles obtained from the borohydride reactions formed relatively dense, irregularly shaped clusters with sizes ranging from 53 to 72 nm.

KEYWORDS: NANOPARTICLE; IRON; ULTRASONIC CAVITATION; SOLUTION PUMPING SPEED; BOROHYDRIDE METHOD.

INTRODUCTION

The significant interest of the scientific and technical community in nanostructured systems stems from their unique properties, structural diversity, and practical applications. Among various nanopowders, iron (Fe) nanoparticles have been widely utilized in science, engineering, and technology. For instance, they serve as effective magnetic adsorbents for soil remediation and wastewater treatment, efficiently removing toxic pollutants [1-10]. Due to their large specific surface area, high adsorption capacity, low cost, environmental safety, and rapid reactivity, Fe nanoparticles are particularly suitable for purifying contaminated water [11]. Additionally, they are used as nano-modifiers in powder metallurgy to produce bulk materials (Fe-based) or as raw materials for 3D metal printing and are applied in many different fields of science and technology [12-16].

Fe nanopowders are typically synthesized using either physical or chemical methods. While physical approaches require expensive equipment, chemical methods often suffer from low productivity and high energy consumption [11, 12]. For example, the chemical-metallurgical method employed by the authors to synthesize

Tien Hiep Nguyen, Nguyen Manh Hung
Department of Materials Science & Engineering,
Le Quy Don Technical University, Hanoi, Vietnam

Ho Thanh Nghi
Viettel Aerospace Institute, Hanoi, Vietnam

Nguyen Van Minh
Institute of Technology, Hanoi, Vietnam

iron-group nanoparticles offers advantages such as scalability at the laboratory level and relatively clean products. However, its efficiency is limited by the slow reduction rate in hydrogen gas during the heat-holding stage. Moreover, excessive reduction temperatures can lead to severe nanoparticle agglomeration, resulting in particles exceeding the nanoscale. Additionally, the multi-step process requires substantial energy input [17-18].

Alternatively, studies have demonstrated that transition metal nanoparticles can be synthesized via the borohydride method. Although fundamentally a chemical approach, this technique offers distinct advantages: it is simple, involves fewer steps, and reduces energy costs by directly converting metal salt solutions into nanoparticles using borohydride (BH_4^-), without the need for high-temperature pyrolysis or multi-stage reduction [19, 20].

Given these findings, the borohydride method is a viable route for synthesizing Fe nanopowders. Although this method has been used, current studies have mostly focused on selecting precursors for the chemical reaction without systematically investigating the simultaneous influence of the pumping speed of the solution and ultrasonic wave amplitude on the size and dispersion of the iron nanoparticles. The novelty of this study resides in the combination of high-amplitude ultrasonic and a high pumping speed of the solution for the synthesis of iron nanoparticles, irrespective of whether the precursor salt is $Fe^{2+}(FeSO_4)$ or $Fe^{3+}(FeCl_3)$. The optimal parameters established in this study allow the method to be scaled up for the preparation of iron nanoparticles beyond the laboratory scale, with fewer intermediate synthesis steps.

MATERIALS AND METHODS

Iron nanoparticles were synthesized via borohydride reduction using two precursor salts: iron (II) sulfate heptahydrate ($FeSO_4 \cdot 7H_2O$) and iron (III) chloride hexahydrate ($FeCl_3 \cdot 6H_2O$). Sodium borohydride ($NaBH_4$) was used as the reducing agent. Prior to the reduction reactions, aqueous solutions of both iron salts (5 wt.%) were freshly prepared.

The experimental setup included a Hielscher UIP1000hd ultrasonic disperser, a pumping system comprising a KNF N 816.3 KT.18 vacuum diaphragm pump and a Heidolph PD 5201 peristaltic pump, together with standard laboratory glassware. A schematic diagram of the synthesis apparatus is presented in figure 1.

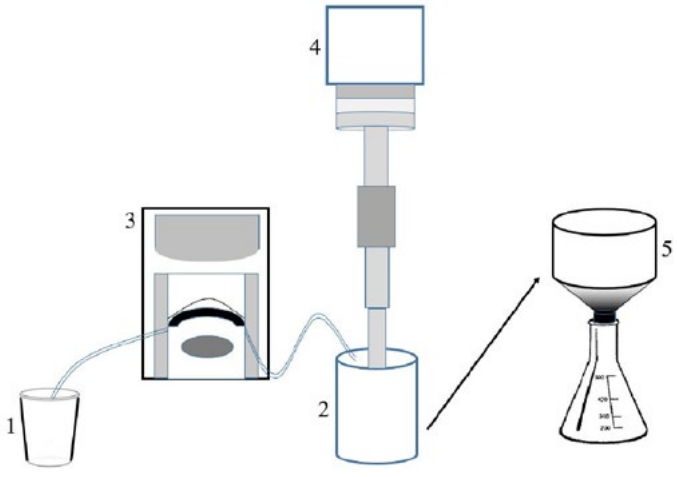

(1) $NaBH_4$ solution; (2) Reactor containing $FeSO_4$/$FeCl_3$ solutions; (3) Pumping system; (4) Ultrasonic disperser; (5) Büchner funnel and flask

Fig.1 -Schematic of iron nanoparticle synthesis by borohydride method.

To optimize the synthesis parameters for iron nanoparticles via the borohydride method, the effects of two process variables were investigated: the pumping speed of the $NaBH_4$ solution - $V(NaBH_4)$ and ultrasonic wave amplitude - A_U. The experimental parameters are summarized in table 1.

Tab.1 - Experimental parameters.

Sample No.		Concentration C ($FeSO_4$), %	Concentration C ($FeCl_3$), %	Concentration C ($NaBH_4$), %	$V(NaBH_4)$, ml/min	A_U, µm
Serie 1	1.1	5		5	3.8	40
	1.2				3.8	80
	1.3				1.9	80
Serie 2	2.1		5	5	3.8	40
	2.2				3.8	80
	2.3				1.9	80

The borohydride reduction reactions proceed according to the following equations:

$$FeSO_4 + 2{\cdot}NaBH_4 + 6{\cdot}H_2O \rightarrow Fe\downarrow + Na_2SO_4 + 2{\cdot}B(OH)_3 + 7{\cdot}H_2\uparrow, \quad (1)$$

$$2{\cdot}FeCl_3 + 6{\cdot}NaBH_4 + 18{\cdot}H_2O \rightarrow 2{\cdot}Fe\downarrow + 6NaCl + 6{\cdot}B(OH)_3 + 21{\cdot}H_2\uparrow, \quad (2)$$

During the synthesis process, ultrasonic mixing was employed to homogenize the reactant solution, as well as to disperse the aggregates of the forming Fe nanoparticles. The resulting precipitate (Fe nanoparticles) was washed with distilled water via the Büchner funnel and flask. Subsequently, the powders were ground using a Fritsch Pulverisette 2 grinder (Germany).

Particle size distributions were determined using dynamic light scattering (Malvern Zetasizer Nano ZS, UK). Specific surface areas were measured via nitrogen adsorption isotherms using the BET method (Nova 1200e analyzer, USA). The average particle diameter (D_a) was calculated from surface area measurements using the formula:

$$D_a = \frac{6}{\rho \cdot S_a}, \quad (3)$$

where ρ represents the theoretical density of iron (7870 kg/m³) and S_a denotes the specific surface area (m²/kg).

Phase composition was analyzed by X-ray diffraction (XRD) using a Difrey-401 diffractometer (Russia) with Cu-Kα radiation. Morphological characterization was performed using scanning electron microscopy (SEM) on a Tescan Vega 3B instrument (Czech Republic).

RESULTS AND DISCUSSION

After preparing six Fe nanoparticle samples (both Series 1 and 2) according to the experimental procedure outlined in table 1, the particle size distribution of these samples was analyzed using dynamic light scattering (DLS). The results are presented in figures 2 and 3.

Analysis of the Fe nanoparticle size distribution diagrams (figures 2 and 3) revealed some important findings, namely: The widest particle distribution was observed in samples №3 (1.3 and 2.3 - with lower solution pumping speed value: $V(NaBH_4)$ = 1.9 ml/min), while samples №2 (1.2 and 2.2 - with higher solution pumping speed value: $V(NaBH_4)$ = 3.8 ml/min and larger ultrasonic wave amplitude A_U = 80 µ) showed the smallest maximum particle size. For both sample series, decreasing the solution pumping speed tended to broaden the particle distribution, while increasing the ultrasonic wave amplitude resulted in smaller maximum particle sizes.

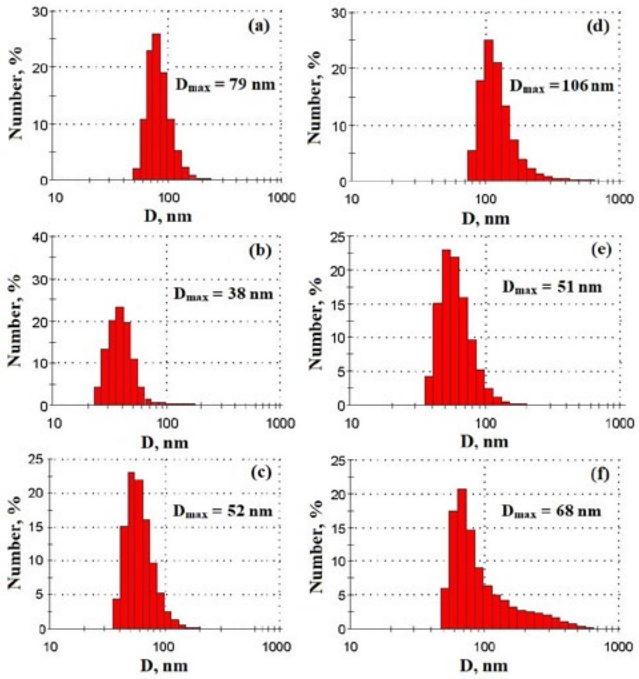

Fig.2 - Plot of the maximum particle size distribution depending on the concentration of $NaBH_4$ samples: 1.1 (a); 1.2 (b); 1.3 (c); 2.1 (d); 2.2 (e); 2.3 (f).

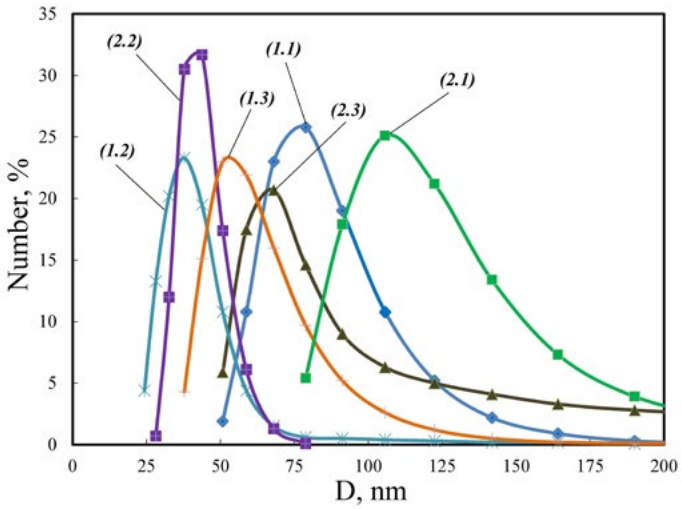

Fig.3 - Particle size distribution graph of the jointly studied samples.

This phenomenon can be attributed to the fact that a high $NaBH_4$ solution pumping speed, when reacting with iron (II) and iron (III) salts, increases the nucleation rate. As a result, more nucleation centers are formed, leading to a larger number of nascent nanoparticles and consequently limiting their growth space, which results in smaller nanoparticles. In the case of high-amplitude ultrasonic waves, the increased energy input likely disrupts crystalline clusters, thereby promoting the formation of smaller particles and enhancing their dispersion.

Moreover, several studies have shown that low-concentration iron salt precursors (5-10 wt.%) are effective for producing metal nanoparticles. However, in borohydride reduction, although a high $NaBH_4$ pumping speed improves reaction kinetics, an excessive amount may lead to an overabundance of $NaBH_4$—an active foaming agent—which increases the viscosity of the solution and impedes crystal nucleation.

Furthermore, the results clearly demonstrate that combining a high-amplitude ultrasonic wave with a high $NaBH_4$ solution pumping speed (samples №2, i.e., 1.2 and 2.2) yields nanoparticles with the most favorable size and disper-

sion in both precursor cases. A comparison between samples №1 (1.1 and 2.1), №2 (1.2 and 2.2) and №3 (1.3 and 2.3) indicates that variations in ultrasonic wave amplitude have a more pronounced impact on particle size than changes in solution pumping speed.

When comparing Series 1 samples (1.1, 1.2, 1.3), synthesized using $FeSO_4$, with Series 2 samples (2.1, 2.2, 2.3), synthesized using $FeCl_3$ as the precursor, it is evident that Series 1 exhibits better nanoparticle size and dispersion. This can be attributed to the fact that the reduction of Fe^{2+} ions (from $FeSO_4$) to metallic iron nanocrystals is more straightforward than the reduction of Fe^{3+} ions (from $FeCl_3$). The reduction of Fe^{3+} to Fe typically proceeds in two steps: the initial formation of Fe^{2+}, followed by the reduction to Fe, as illustrated in the reactions below:

$$Fe^{3+} + e \rightarrow Fe^{2+} \quad (4)$$

$$Fe^{2+} + 2e \rightarrow Fe \quad (5)$$

Based on the evaluation of the particle size distribution graphs of the synthesized nanoparticles, samples №2 (1.2 and 2.2), representing both iron (II) and iron (III) salt precursors, were selected for further characterization studies, as they exhibited the best dispersion and particle size distribution. The XRD results of these two samples, along with elemental analysis by EDX from SEM images, are presented in figure 4.

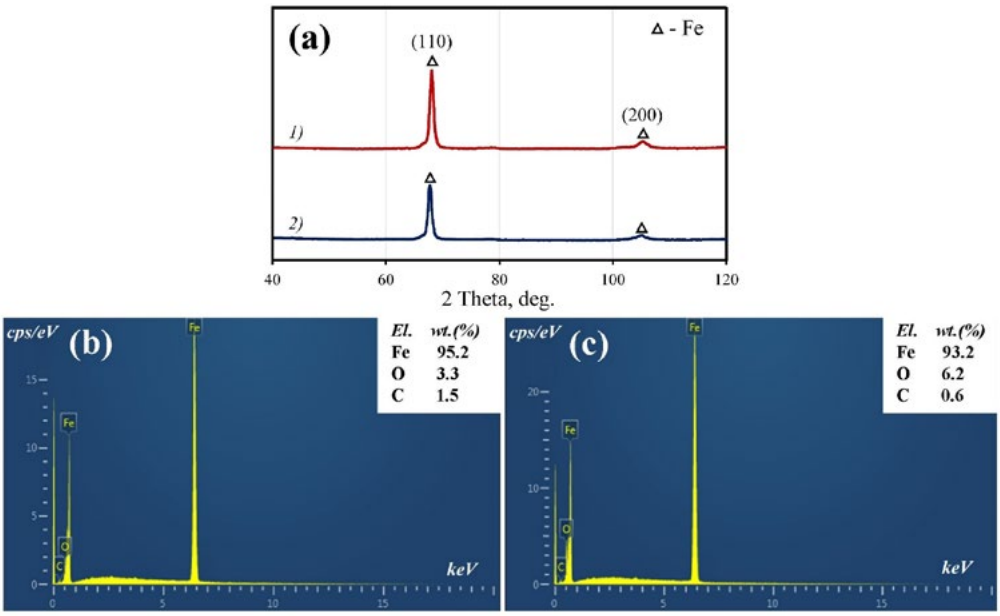

(a1, b) Sample 1.2; (a2, c) Sample 2.2

Fig.4 - The XRD patterns and elemental analysis by EDX of the samples.

Results from the XRD analysis (figure 4a) show diffraction peaks corresponding to the (110) and (200) planes of the pure α-Fe metallic phase, in accordance with JCPDS file no. 65-4899. No additional phases or impurities were detected in the XRD patterns.

Elemental analysis by the EDX from SEM image data (figures 4b, 4c) reveals a small amount of carbon in the samples, which is attributed to the carbon substrate used during sample preparation. A detectable amount of oxygen (ranging from 3.3% to 6.2%) is also present. This is expected, as a small portion of Fe nanoparticles can oxidize during the borohydride synthesis process when no inert gas environment is maintained.

The presence of oxygen detected by the EDX, coupled with its absence in the XRD analysis, suggests that the oxide layer formed during synthesis is either amorphous or present as an extremely thin crystalline layer. Consequently, this layer lacks sufficient structural order to generate detectable diffraction peaks in the XRD pattern [21-23].

SEM images of the two nanoparticle samples (1.2 and 2.2), synthesized via the borohydride method from iron (II) and iron (III) salt solutions, respectively, along with their particle size distributions (derived from SEM image data), are presented in figure 5. In addition, the specific surface area analysis and the corresponding calculated particle sizes (based on these measurements) are summarized in table 2.

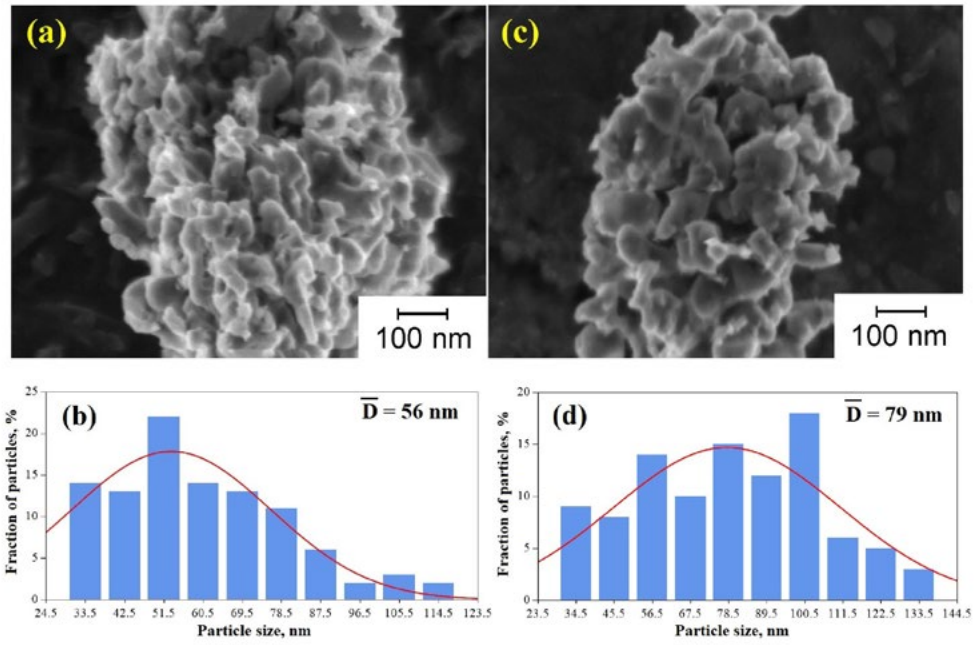

(a, b) Sample 1.2; (c, d) Sample 2.2

Fig.5 - SEM-images and Particle size distribution of the samples.

Tab.2 - Specific surface area and particle size calculation results.

Sample	S_a, m^2/g	D_a, nm	D_{SEM}, nm	|D|, nm	$D_{max(DLS),}$ nm
№ 1.2 ($FeSO_4$ + $NaBH_4$)	15.5 ± 0.8	49 ± 2	56 ± 3	53 ± 3	38 ± 2
№ 2.2 ($FeCl_3$ + $NaBH_4$)	11.9 ± 0.6	64 ± 3	79 ± 4	72 ± 4	51 ± 3

In both cases, the obtained Fe nanoparticles form relatively dense clusters with undefined shapes. When reducing the iron (II) salt solution ($FeSO_4$) using the borohydride method, the resulting nanoparticles have a smaller average size (53 nm) compared to those obtained from the reduction of the iron (III) salt solution ($FeCl_3$), which average around 72 nm.

Although DLS typically measures larger hydrodynamic diameters due to the inclusion of the solvation layer, the observed differences between $D_{max(DLS)}$ and D_{BET}/D_{SEM} in this study can be rationalized as follows. DLS is conducted on suspensions prepared by dispersing the powder in a liquid using high-intensity ultrasound, which breaks down clusters into individual particles or small agglomerates, leading to smaller recorded sizes. Conversely, BET and SEM are performed on dry powder samples, where drying and grinding promote aggregation into larger, dense clusters, resulting in larger measured diameters. Hence, the results are fully consistent with one another.

CONCLUSIONS

Six iron nanoparticle samples, divided into two series, were synthesized via the borohydride method using two different precursors ($FeSO_4$ and $FeCl_3$), with variations in solution pumping speed and ultrasonic wave amplitude.

It was found that the combination of a high-amplitude ultrasonic wave and a high $NaBH_4$ solution pumping speed yielded nanoparticles with optimal size and dispersion in both cases.

When iron (II) sulfate ($FeSO_4$) was used as the precursor, the resulting nanoparticles exhibited better size and dispersion compared to those synthesized from iron (III) chloride ($FeCl_3$).

In both cases, the Fe nanoparticles obtained via the borohydride reduction formed relatively dense clusters with irregular shapes, and their sizes ranged from 53 to 72 nm.

REFERENCES

[1] B. Bhushan, Springer Handbook of Nanotechnology, 4th edition. Springer Berlin Heidelberg, Germany, 1500 p., 2017.
[2] D. I. Ryzhonkov, V. V. Levina, E. L. Dzidziguri, Nanomaterialy: Uchebnoe posobie (Nanomaterials: Textbook), Moscow: BINOM, Laboratoriya Znanii, Russia, 365 p., 2008.
[3] V. Tavallali, M. Kiani, S. Hojati, "Iron nano-complexes and iron chelate improve biological activities of sweet basil (Ocimum basilicum L.)," Plant Physiology and Biochemistry, 2019, vol. 144, p. 445. https://doi.org/10.1016/j.plaphy.2019.10.021
[4] Ł. Nagi, A. Płużek, "Electrical Strength of Natural Esters Doped by Iron Nanopowder in a Hydrophobic Carbon Shell," Materials, 2020, vol. 13, art. 1956. https://doi.org/10.3390/ma13081956
[5] Y. P. Sun, X. Li, J. Cao, W. X. Zhang, H. P. Wang, "Characterization of zero-valent iron nanoparticles," Advances in Colloid and Interface Science, 2006, vol. 120 (1-3), p. 47. https://doi.org/10.1016/j.cis.2006.03.001
[6] Q. J. Rasheed, K. Pandian, K. Muthukumar, "Treatment of petroleum refinery wastewater by ultrasounddispersed nanoscale zero-valent iron particles," Ultrasonics Sonochemistry, 2011, vol. 18(5), p. 1138. https://doi.org/10.1016/j.ultsonch.2011.03.015
[7] S. S. Chen, D. H. Hong, C. W. Li, "A new method to produce nanoscale iron for nitrate removal," Journal of Nanoparticle Research, 2005, vol. 6, p. 639. https://doi.org/10.1007/s11051-004-6672-2
[8] J. Noma, H. Abe, T. Kikuchi, J. Furusho, M. Naito, "Magnetorheology of colloidal dispersion containing Fe nanoparticles synthesized by arc-plasma method," Journal of Magnetism and Magnetic Materials, 2010, no. 322, p. 1868. https://doi.org/10.1016/j.jmmm.2009.12.043
[9] S. Veintemillas-Verdaguer, O. Bomati, M. P. Morales, P. E. Di Nunzio, S. Martelli, "Iron ultrafine nanoparticles prepared by aerosol laser pyrolysis," Materials Letters, 2003, vol. 57(5-6), p. 1184. https://doi.org/10.1016/S0167-577X(02)00953-9
[10] M. Bystrzejewski, "Synthesis of carbon-encapsulated iron nanoparticles via solid state reduction of iron oxide nanoparticles," Journal of Solid State Chemistry, 2011, vol. 184(6), p. 1492. https://doi.org/10.1016/j.jssc.2011.04.018
[11] T. H. Nguyen, V. M. Nguyen, "Kinetics of synthesizing process for obtaining iron nanopowder by chemical-metallurgical method under isothermal conditions," Chernye Metally, 2021, no. 1, p. 72. https://doi.org/10.17580/chm.2021.01.11
[12] T. H. Nguyen, V. M. Nguyen, M. H. Nguyen, V. N. Danchuk, "Preparation procedure to obtain iron nanopowder under non-isothermal conditions," Journal of the Belarusian State University Chemistry, 2021, no. 1, p. 28. https://doi.org/10.33581/2520-257X-2021-1-28-35
[13] W. X. Zhang, "Nanoscale Iron Particles for Environmental Remediation: An Overview," Journal of Nanoparticle Research, 2003, vol. 5, p. 323. https://doi.org/10.1023/A:1025520116015
[14] V. M. Nguyen, G. Karunakaran, T. H. Nguyen, E. A. Kolesnikov, M. I. Alymov, V. V. Levina, Y. V. Konyukhov, "Enhancement of structural and mechanical properties of Fe+0.5%C steel powder alloy via incorporation of Ni and Co nanoparticles," Letters on Materials, 2020, vol. 10, no. 2, p. 174. https://doi.org/10.22226/2410-3535-2020-2-174-178
[15] T. H. Nguyen, V. M. Nguyen "The effect of surfactants on the particle size of iron, cobalt and nickel nanopowders," Powder Metallurgy and Functional Coatings, 2020, no. 1, p. 22. https://doi.org/10.17073/1997-308X-2020-22-28
[16] A. Koshanova, G. Partizan, B. Mansurov, B. Medyanova, M. Mansurova, B. Aliev, X. Jiang, "Synthesis of carbon nanostructures on iron nanopowders," Journal of Physics: Conference Series, 2016, vol. 741, no. 012017. https://doi.org/10.1088/1742-6596/741/1/012017
[17] V. M. Nguyen, T. H. Nguyen, "Investigation of the Process of Synthesizing Nanosized Nickel Powders by Hydrogen Reduction under Nonisothermal Conditions," Metallurgist, 2021, vol. 65(1-2), p. 206. https://doi.org/10.1007/s11015-021-01149-2
[18] T. H. Nguyen, N. V. Minh, V. N. Danchuk, M. H. Nguyen, H. V. Nguyen, X. D. Tang, "Kinetic Characteristics of the Process of Synthesis of Nickel Nanopowder by the Chemical Metallurgy Method," Nanotechnologies in Russia, 2020, vol. 15(2), p. 146. https://doi.org/10.1134/S1995078020020160
[19] Y. V. Konyukhov, "Heavy-Metal Extraction from Wastewater by Means of Iron Nanopowder," Steel in Translation, 2018, 48(2), p. 135. https://doi.org/10.3103/S0967091218020080
[20] A. A. Kuzharov, A. A. Milov, Y. S. Gerasina, I. Yu. Neverov, M. S. Lipkin, V. M. Lipkin, A. S. Kolomiitsev, A. A. Fedotov, M. A. Soldatov, A. V. Soldatov, "The Influence of Stabilizer on the Formation and Tribotechnical Properties of Cu Nanoparticles," Protection of Metals and Physical Chemistry of Surfaces, 2019, vol. 55, p. 283. https://doi.org/10.1134/S2070205119020151
[21] L. M. Moreau, D. H. Ha, H. Zhang, R. Hovden, D. A. Muller, R. D. Robinson, "Defining Crystalline/Amorphous Phases of Nanoparticles through X-ray Absorption Spectroscopy and X-ray Diffraction: The Case of Nickel Phosphide," Chemistry of Materials, 2013, vol. 25 (12), p. 2394. https://doi.org/10.1021/cm303490
[22] E. V. Zakharova, E. L. Dzidziguri, E. N. Sidorova, A. A. Vasiliev, I. A. Pelevin, D. Y. Ozherelkov, A. Y. Nalivaiko, A. A. Gromov, "Characterization of Multiphase Oxide Layer Formation on Micro and Nanoscale Iron Particles," Metals, 2021, vol. 11(1), art. 12, https://doi.org/10.3390/met11010012
[23] S. Muthukrishnan, S. Bhakya, V. Ramalingam, "Metal nanoparticles synthesis: an overview of different synthesis methods, mode of action and their biomedical application," Discover Applied Sciences, 2025, vol. 7, art. 1079. https://doi.org/10.1007/s42452-025-07210-y

TORNA ALL'INDICE >